Comparison between the P_ψ^N and $P_{\psi s}^\Lambda$ systems

Kan Chen,[*] Zi-Yang Lin,[†] and Shi-Lin Zhu[‡]

School of Physics and Center of High Energy Physics, Peking University, Beijing 100871, China

(Received 13 November 2022; accepted 8 December 2022; published 27 December 2022)

We construct the effective potentials of the P_ψ^N and $P_{\psi s}^\Lambda$ states based on the $\mathrm{SU}(3)_\mathrm{f}$ symmetry and heavy quark symmetry. Then we perform the coupled-channel analysis of the lowest-isospin P_ψ^N and $P_{\psi s}^\Lambda$ systems. The coupled-channel effects play different roles in the P_ψ^N and $P_{\psi s}^\Lambda$ systems. In the P_ψ^N systems, this effect gives minor corrections to the masses of the P_ψ^N states. In the $P_{\psi s}^\Lambda$ system, the $\Lambda_c\bar{D}_s - \Xi_c\bar{D}$ coupling will shift the mass of the $P_{\psi s}^\Lambda(4338)^0$ close to the $\Xi_c\bar{D}$ threshold. The $\Lambda_c\bar{D}_s^{(*)} - \Xi_c\bar{D}^{(*)}$ coupling will also produce extra $P_{\psi s}^\Lambda$ states. We discuss the correspondence between the P_ψ^N and $P_{\psi s}^\Lambda$ states. Our results prefer that the SU(3) partners of the observed $P_\psi^N(4312)^+$, $P_\psi^N(4440)^+$, and $P_\psi^N(4457)^+$ in the $P_{\psi s}^\Lambda$ system not have been found yet.

DOI: 10.1103/PhysRevD.106.116017

I. INTRODUCTION

Very recently, the LHCb Collaboration announced the observation of a $P_{\psi s}^\Lambda(4338)^0$ signal[1] from the $J/\Psi\Lambda$ mass spectrum in the $B^- \to J/\Psi\Lambda\bar{p}$ process [2]. The mass and width of this new pentaquark candidate were measured to be

$$M_{P_{cs}} = 4338.2 \pm 0.7 \pm 0.4 \text{ MeV}, \tag{1}$$

$$\Gamma_{P_{cs}} = 7.0 \pm 1.2 \pm 1.3 \text{ MeV}. \tag{2}$$

Meanwhile, the amplitude analysis prefers the $\frac{1}{2}^-$-spin-parity quantum numbers. The central value of the mass of $P_{\psi s}^\Lambda(4338)^0$ is above the $\Xi_c\bar{D}$ threshold. Thus, this state cannot be directly assigned as the $\Xi_c\bar{D}$ molecular state. However, the authors of Ref. [3] pointed out that the line shape of this resonance could be distorted from the conventional Breit-Wigner distribution if it lies very close to and strongly couples to the threshold.

Besides the newly observed $P_{\psi s}^\Lambda(4338)^0$, the $P_{\psi s}^\Lambda(4459)^0$ was observed at LHCb [4] as a candidate of a $\Xi_c\bar{D}^*$ molecular state, which agrees well with the prediction from the chiral effective field theory in Ref. [5]. The strange hidden-charm states were also discussed in Refs. [6–14] and reviewed extensively in Refs. [15–20].

The mass of the $P_{\psi s}^\Lambda(4459)^0$ is about 19 MeV below the $\Xi_c\bar{D}$ threshold. In Ref. [21], the author argued that from heavy quark symmetry, the $[\Xi_c\bar{D}]^{1/2^-}$, $[\Xi_c\bar{D}^*]^{1/2^-}$, and $[\Xi_c\bar{D}^*]^{3/2^-}$ channels should share identical potentials and have comparable binding energies. However, since the mass of the charm quark is not heavy enough, a serious study on the masses of the $[\Xi_c\bar{D}^*]^{1/2^-}/[\Xi_c\bar{D}^*]^{3/2^-}$ states should also take the heavy quark symmetry-breaking effect into account. With the assignment of the $P_{\psi s}^\Lambda(4338)^0$ and $P_{\psi s}^\Lambda(4459)^0$ as the $[\Xi_c\bar{D}]^{1/2^-}$ and $[\Xi_c\bar{D}^*]^{1/2^-}$ ($[\Xi_c\bar{D}^*]^{3/2^-}$) molecular states, the degeneracy of the $[\Xi_c\bar{D}^*]^{1/2^-}$ and $[\Xi_c\bar{D}^*]^{3/2^-}$ channels is removed by the coupled-channel effects and recoil corrections.

Another novel phenomenon from the $M_{J/\Psi\Lambda}$ invariant spectrum [2] is that there seems to be a structure around $M = 4254$ MeV. To understand this signal, the LHCb checked the $m(J/\Psi\Lambda)$ distribution close to the $\Lambda_c^+ D_s^-$ threshold and found that this signal is not statistically significant. Nevertheless, the authors in Ref. [22] investigated the $P_{\psi s}^\Lambda(4338)^0$ and $P_{\psi s}^\Lambda(4255)^0$ pole positions from a unitary $\Xi_c\bar{D} - \Lambda_c\bar{D}_s$ coupled-channel scattering amplitude. Besides this, the $P_{\psi s}^\Lambda(4255)^0$ pole was also found in a model with the coupling between the meson-baryon molecule and the compact five-quark state [23]. The $P_{\psi s}^\Lambda(4255)^0$ state was also suggested in an effective field theory framework [24].

The analogy between the observed $[P_\psi^N(4312)^+$, $P_\psi^N(4440)^+$, $P_\psi^N(4457)^+]$ [25,26] and $[P_{\psi s}^\Lambda(4338)^0$, $P_{\psi s}^\Lambda(4459)]$ states is discussed in Refs. [27–29]. However,

[*]chenk_10@pku.edu.cn
[†]lzy_15@pku.edu.cn
[‡]zhusl@pku.edu.cn

[1]We adopt the nomenclature proposed by the LHCb Collaboration [1] throughout this paper.

since the Σ_c and Ξ_c belong to different $\mathrm{SU}(3)_\mathrm{f}$ multiplets, the relations between the discussed P_ψ^N and $P_{\psi s}^\Lambda$ states are not clear. Besides, the $P_{\Psi ss}^N$ pentaquark states as the partners of the P_ψ^N and $P_{\psi s}^\Lambda$ states are investigated in Ref. [30].

If the $P_{\psi s}^\Lambda$ states and P_ψ^N states can be related via $\mathrm{SU}(3)_\mathrm{f}$ symmetry, it is important to investigate the similarities and differences between these two sets of molecular candidates. In Refs. [31,33], we discussed the symmetry properties of different heavy-flavor molecular systems via a quark-level Lagrangian. We proposed that the interactions of different heavy-flavor molecules can be related via a generalized flavor-spin symmetry [31]. This framework provides a suitable tool to discuss the similarities between the P_ψ^N and $P_{\psi s}^\Lambda$ states.

We also notice an important difference between the P_ψ^N and $P_{\psi s}^\Lambda$ states. The minimal quark components of the P_ψ^N and $P_{\psi s}^\Lambda$ states are $c\bar{c}nnn$ (a calculation based on the compact pentaquark configuration of the P_ψ^N states can be found in Ref. [32]) and $c\bar{c}nns$ ($n = u, d$), respectively. For the charmed/charmed-strange mesons and baryons, the $\mathrm{SU}(3)_\mathrm{f}$ symmetry-breaking effects are reflected on their physical masses, and we need to distinguish the s quark from u, d quarks when we study the $P_{\psi s}^\Lambda$ systems. Unlike the P_ψ^N pentaquarks, the $P_{\psi s}^\Lambda$ states can couple to two sets of channels—i.e., the $cns - \bar{c}n$-type and $cnn - \bar{c}s$-type channels. In Table I, we list the possible open-charm channels and their thresholds for the P_ψ^N and $P_{\psi s}^\Lambda$ systems.

In this work, we will take $P_{\psi s}^\Lambda(4338)^0$ as a molecular candidate and discuss the following three issues:

(1) Can we understand the minor binding energy of the $P_{\psi s}^\Lambda(4338)^0$ (close to the $\Xi_c\bar{D}$ threshold) through a $\Xi_c\bar{D} - \Lambda_c\bar{D}_s$ coupled-channel effect?
(2) Can we produce a $P_{\psi s}^\Lambda(4255)^0$ bound state by including the $\Xi_c\bar{D} - \Lambda_c\bar{D}_s$ coupled-channel effect with the potential constrained from $\mathrm{SU}(3)_\mathrm{f}$ symmetry?
(3) What is the correspondence between the P_ψ^N and $P_{\psi s}^\Lambda$ states if the interactions of the P_ψ^N and $P_{\psi s}^\Lambda$ states obey a generalized flavor-spin symmetry?

TABLE I. The thresholds of the meson-baryon channels associated with the P_ψ^N and $P_{\psi s}^\Lambda$ systems. We adopt the isospin averaged masses for the ground charmed mesons and baryons [34]. All values are in units of MeV.

P_ψ^N			$P_{\psi s}^\Lambda$		
$\Lambda_c\bar{D}$	4153.7	$\Lambda_c\bar{D}_s$	4255.5	$\Xi_c\bar{D}$	4336.7
$\Lambda_c\bar{D}^*$	4295.0	$\Lambda_c\bar{D}_s^*$	4398.7	$\Xi_c\bar{D}^*$	4478.0
$\Sigma_c\bar{D}$	4320.8	$\Sigma_c\bar{D}_s$	4422.5	$\Xi_c'\bar{D}$	4446.0
$\Sigma_c^*\bar{D}$	4385.4	$\Sigma_c^*\bar{D}_s$	4487.1	$\Xi_c^*\bar{D}$	4513.2
$\Sigma_c\bar{D}^*$	4462.1	$\Sigma_c\bar{D}_s^*$	4565.7	$\Xi_c'\bar{D}^*$	4587.4
$\Sigma_c^*\bar{D}^*$	4526.7	$\Sigma_c^*\bar{D}_s^*$	4630.3	$\Xi_c^*\bar{D}^*$	4654.5

This paper is organized as follows: We present our theoretical framework in Sec. II and the corresponding numerical results and discussions in Sec. III. Section IV is the summary.

II. FRAMEWORK

In Ref. [33], we proposed an isospin criterion and pointed out that the P_ψ^N and $P_{\psi s}^\Lambda$ states with the lowest isospin numbers are more likely to form bound states. Based on the same Lagrangian, we only focus on the P_ψ^N and $P_{\psi s}^\Lambda$ states with isospin numbers $I = 1/2$ and 0, respectively. Thus, we will not include the $\Sigma_c^{(*)}\bar{D}_s^{(*)}$ channels listed in Table I for the $P_{\psi s}^\Lambda$ system.

For the $I = 1/2$ P_ψ^N states, we consider the following channels for the $J = 1/2$ and $3/2$ states:

$$J = \frac{1}{2} : \Lambda_c\bar{D}, \Lambda_c\bar{D}^*, \Sigma_c\bar{D}, \Sigma_c\bar{D}^*, \Sigma_c^*\bar{D}^*, \tag{3}$$

$$J = \frac{3}{2} : \Lambda_c\bar{D}^*, \Sigma_c^*\bar{D}, \Sigma_c\bar{D}^*, \Sigma_c^*\bar{D}^*. \tag{4}$$

Similarly, for the $I = 0$ $P_{\psi s}^\Lambda$ states, we include the following channels for the $J = 1/2$ and $3/2$ states:

$$J = \frac{1}{2} : \Lambda_c\bar{D}_s, \Lambda_c\bar{D}_s^*, \Xi_c\bar{D}, \Xi_c\bar{D}^*, \Xi_c'\bar{D}, \Xi_c'\bar{D}^*, \Xi_c^*\bar{D}^*, \tag{5}$$

$$J = \frac{3}{2} : \Lambda_c\bar{D}_s^*, \Xi_c\bar{D}^*, \Xi_c^*\bar{D}, \Xi_c'\bar{D}^*, \Xi_c^*\bar{D}^*. \tag{6}$$

The result of the P_ψ^N ($P_{\psi s}^\Lambda$) state with $J = 5/2$ can be obtained from a single-channel calculation and was predicted in Ref. [33] in the same framework. Thus, we will not discuss them further in this work.

A. Lagrangians for the baryon-meson systems

To describe the S-wave interactions between the ground charmed/charmed-strange baryons and mesons, we introduce the following quark-level Lagrangian [5,33,35,36]:

$$\mathcal{L} = g_s\bar{q}\mathcal{S}q + g_a\bar{q}\gamma_\mu\gamma^5\mathcal{A}^\mu q. \tag{7}$$

Here, $q = (u, d, s)$, and g_s and g_a are two independent coupling constants that describe the interactions from the exchanges of the scalar and axial-vector meson currents. They encode the nonperturbative low-energy dynamics of the considered heavy-flavor meson-baryon systems.

From this Lagrangian, the effective potential of the light quark-quark interactions reads

$$\mathcal{V} = \tilde{g}_s\boldsymbol{\lambda}_1\cdot\boldsymbol{\lambda}_2 + \tilde{g}_a\boldsymbol{\lambda}_1\cdot\boldsymbol{\lambda}_2\boldsymbol{\sigma}_1\cdot\boldsymbol{\sigma}_2. \tag{8}$$

Here,

$$\boldsymbol{\lambda}_1\cdot\boldsymbol{\lambda}_2=\lambda_1^8\lambda_2^8+\lambda_1^i\lambda_2^i+\lambda_1^j\lambda_2^j, \tag{9}$$

where i and j sum from 1 to 3 and 4 to 7, respectively. The operators $\lambda_1^8\lambda_2^8$ $(\lambda_1^8\lambda_2^8(\boldsymbol{\sigma}_1\cdot\boldsymbol{\sigma}_2))$, $\lambda_1^i\lambda_2^i$ $(\lambda_1^i\lambda_2^i(\boldsymbol{\sigma}_1\cdot\boldsymbol{\sigma}_2))$, and $\lambda_1^j\lambda_2^j$ $(\lambda_1^j\lambda_2^j(\boldsymbol{\sigma}_1\cdot\boldsymbol{\sigma}_2))$ arise from the exchanges of the isospin singlet, triplet, and two doublet light scalar (axial-vector) meson currents, respectively. The redefined coupling constants are $\tilde{g}_s\equiv g_s^2/m_{\mathcal{S}}^2$ and $\tilde{g}_a\equiv g_a^2/m_{\mathcal{A}}^2$.

The Lagrangian in Eq. (7) allows the exchanges of two types of scalar and axial-vector mesons that have quantum numbers $I(J^P)=0(0^+)$, $1(0^+)$, $1/2(0^+)$ and $I(J^P)=0(1^+)$, $1(1^+)$, $1/2(1^+)$, respectively. At present, we cannot specifically pin down the coupling parameter of each exchanged meson in the above six meson currents. Alternatively, since the mesons in each meson current have identical interacting Lorentz structure, we use the coupling constant $\tilde{g}_s$ $(\tilde{g}_a)$ to collectively absorb the total dynamical effects from the exchange of each scalar (axial-vector) meson current. In addition, the couplings $\tilde{g}_s$ $(\tilde{g}_a)$ for the scalar (axial-vector) meson currents with different isospin numbers are the same in the SU(3) limit.

The effective potential between the ith baryon-meson channel B_iM_i and the jth baryon-meson channel B_jM_j with total isospin I and total angular momentum J can be calculated as

$$v_{ij}=\langle[B_iM_i]_J^I|\mathcal{V}|[B_jM_j]_J^I\rangle. \tag{10}$$

Here, $|[B_iM_i]_J^I\rangle$ is the quark-level flavor-spin wave function of the considered ith-channel baryon-meson system

$$|[B_iM_i]_J^I\rangle=\sum_{m_{I_1},m_{I_2}}C^{I,I_z}_{I_1,m_{I_1};I_2,m_{I_2}}\phi^{B_{if}}_{I_1,m_{I_1}}\phi^{M_{if}}_{I_2,m_{I_2}}\otimes\sum_{m_{S_1},m_{S_2}}C^{J,J_z}_{S_1,m_{S_1};S_2,m_{S_2}}\phi^{B_{is}}_{S_1,m_{S_1}}\phi^{M_{is}}_{S_2,m_{S_2}}. \tag{11}$$

In Eq. (11), $\phi^{B_{is}}_{S_1,m_{S_1}}$ and $\phi^{M_{is}}_{S_2,m_{S_2}}$ are the spin wave functions of the baryon and meson, respectively. The total spin wave function can be obtained with the help of SU(2) CG coefficient $C^{J,J_z}_{S_1,m_{S_1};S_2,m_{S_2}}$. For the flavor wave functions of the considered baryons $(\phi^{B_{if}}_{I_1,m_{I_1}})$ and mesons $(\phi^{M_{if}}_{I_1,m_{I_1}})$, their explicit forms have been given in Ref. [31]. When constructing the total flavor wave functions of the considered baryon-meson systems, we use the SU(2) CG coefficient and take the s quark as a flavor singlet.

The coupled-channel Lippmann-Schwinger equation (LSE) reads

$$\mathbb{T}(E)=\mathbb{V}+\mathbb{V}\mathbb{G}(E)\mathbb{T}(E), \tag{12}$$

with

$$\mathbb{V}=\begin{pmatrix}v_{11}&\cdots&v_{1i}&\cdots&v_{1n}\\ \vdots&&\vdots&&\vdots\\ v_{j1}&\cdots&v_{ji}&\cdots&v_{jn}\\ \vdots&&\vdots&&\vdots\\ v_{n1}&\cdots&v_{ni}&\cdots&v_{nn}\end{pmatrix}, \tag{13}$$

$$\mathbb{T}(E)=\begin{pmatrix}t_{11}(E)&\cdots&t_{1i}(E)&\cdots&t_{1n}(E)\\ \vdots&&\vdots&&\vdots\\ t_{j1}(E)&\cdots&t_{ji}(E)&\cdots&t_{jn}(E)\\ \vdots&&\vdots&&\vdots\\ t_{n1}(E)&\cdots&t_{ni}(E)&\cdots&t_{nn}(E)\end{pmatrix}, \tag{14}$$

and

$$\mathbb{G}(E)=\mathrm{diag}\{G_1(E),\ldots,G_i(E),\ldots,G_n(E)\}. \tag{15}$$

Here,

$$G_i=\frac{1}{2\pi^2}\int dq\frac{q^2}{E-\sqrt{m_{i1}^2+q^2}-\sqrt{m_{i2}+q^2}}u^2(\Lambda). \tag{16}$$

Here, m_{i1} and m_{i2} are the masses in the ith channel of the baryon and meson, respectively. In our previous work [31,33], we use a step function to exclude the contributions from higher momenta to perform the single-channel calculation. In the coupled-channel case, we need to further suppress the contributions from the channels that are far away from the thresholds of the considered channels. Thus, we introduce a dipole form factor $u(\Lambda)=(1+q^2/\Lambda^2)^{-2}$ with regular parameter $\Lambda=1.0$ GeV [22,37,38].

The pole position of Eq. (12) satisfies $||\mathbf{1}-\mathbb{V}\mathbb{G}||=0$. For the bound state below the lowest channel, we search the bound-state solution in the first Riemann sheet of the lowest channel. For the quasibound state between the thresholds of the ith and jth channels, we adopt the complex scaling method and replace the integration variable q with $q\to q\times\exp(-i\theta)$ while maintaining $0<\theta<\pi/2$ to find the quasibound-state solution in the first Riemann sheet of the higher jth channel and the second Riemann sheet of the lower ith channel. [39].

III. NUMERICAL RESULTS

A. Determination of $\tilde{g}_s$ and $\tilde{g}_a$

We first determine the parameters $\tilde{g}_s$ and $\tilde{g}_a$ in our model. We collect the matrix elements of $\langle\boldsymbol{\lambda}_1\cdot\boldsymbol{\lambda}_2\rangle$, $\langle\boldsymbol{\lambda}_1\cdot\boldsymbol{\lambda}_2\boldsymbol{\sigma}_1\cdot\boldsymbol{\sigma}_2\rangle$ for the P_ψ^N and $P_{\psi s}^\Lambda$ states in Tables II and III, respectively.

We can directly obtain the effective potentials associated with the P_ψ^N and $P_{\psi s}^\Lambda$ states from Tables II and III,

TABLE II. The matrix elements of $[\langle \boldsymbol{\lambda}_1 \cdot \boldsymbol{\lambda}_2 \rangle, \langle \boldsymbol{\lambda}_1 \cdot \boldsymbol{\lambda}_2 \boldsymbol{\sigma}_1 \cdot \boldsymbol{\sigma}_2 \rangle]$ for the meson-baryon channels associated with the $J^P = 1/2^-$ and $3/2^-$ P_ψ^N systems.

$\mathbb{V}_{1/2}^{P_\psi^N}$						$\mathbb{V}_{3/2}^{P_\psi^N}$				
Channel	$\Lambda_c\bar{D}$	$\Lambda_c\bar{D}^*$	$\Sigma_c\bar{D}$	$\Sigma_c\bar{D}^*$	$\Sigma_c^*\bar{D}^*$	Channel	$\Lambda_c\bar{D}^*$	$\Sigma_c^*\bar{D}$	$\Sigma_c\bar{D}^*$	$\Sigma_c^*\bar{D}^*$
$\Lambda_c\bar{D}$	$[\frac{2}{3}, 0]$	$[0, 0]$	$[0, 0]$	$[0, 2\sqrt{3}]$	$[0, 2\sqrt{6}]$	$\Lambda_c\bar{D}^*$	$[\frac{2}{3}, 0]$	$[0, -2\sqrt{3}]$	$[0, 2]$	$[0, 2\sqrt{5}]$
$\Lambda_c\bar{D}^*$		$[\frac{2}{3}, 0]$	$[0, 2\sqrt{3}]$	$[0, -4]$	$[0, 2\sqrt{2}]$	$\Sigma_c^*\bar{D}$		$[-\frac{10}{3}, 0]$	$[0, -\frac{10}{3\sqrt{3}}]$	$[0, -\frac{10\sqrt{\frac{5}{3}}}{3}]$
$\Sigma_c\bar{D}$			$[-\frac{10}{3}, 0]$	$[0, -\frac{20}{3\sqrt{3}}]$	$[0, \frac{10\sqrt{\frac{2}{3}}}{3}]$	$\Sigma_c\bar{D}^*$			$[-\frac{10}{3}, -\frac{20}{9}]$	$[0, \frac{10\sqrt{5}}{9}]$
$\Sigma_c\bar{D}^*$				$[-\frac{10}{3}, \frac{40}{9}]$	$[0, \frac{10\sqrt{2}}{9}]$	$\Sigma_c^*\bar{D}^*$				$[-\frac{10}{3}, \frac{20}{9}]$
$\Sigma_c^*\bar{D}^*$					$[-\frac{10}{3}, \frac{50}{9}]$					

TABLE III. The matrix elements of $[\langle \boldsymbol{\lambda}_1 \cdot \boldsymbol{\lambda}_2 \rangle, \langle \boldsymbol{\lambda}_1 \cdot \boldsymbol{\lambda}_2 \boldsymbol{\sigma}_1 \cdot \boldsymbol{\sigma}_2 \rangle]$ for the meson-baryon channels associated with the $J^P = 1/2^-$ and $3/2^-$ $P_{\psi s}^\Lambda$ systems.

$\mathbb{V}_{1/2}^{P_{cs}}$								$\mathbb{V}_{3/2}^{P_{cs}}$					
Channel	$\Lambda_c\bar{D}_s$	$\Lambda_c\bar{D}_s^*$	$\Xi_c\bar{D}$	$\Xi_c\bar{D}^*$	$\Xi_c'\bar{D}$	$\Xi_c'\bar{D}^*$	$\Xi_c^*\bar{D}^*$	Channel	$\Lambda_c\bar{D}_s^*$	$\Xi_c\bar{D}^*$	$\Xi_c^*\bar{D}$	$\Xi_c'\bar{D}^*$	$\Xi_c^*\bar{D}^*$
$\Lambda_c\bar{D}_s$	$[-\frac{4}{3}, 0]$	$[0, 0]$	$[2\sqrt{2}, 0]$	$[0, 0]$	$[0, 0]$	$[0, 2\sqrt{2}]$	$[0, 4]$	$\Lambda_c\bar{D}_s^*$	$[-\frac{4}{3}, 0]$	$[2\sqrt{2}, 0]$	$[0, -2\sqrt{2}]$	$[0, 2\sqrt{\frac{2}{3}}]$	$[0, 2\sqrt{\frac{10}{3}}]$
$\Lambda_c\bar{D}_s^*$		$[-\frac{4}{3}, 0]$	$[0, 0]$	$[2\sqrt{2}, 0]$	$[0, 2\sqrt{2}]$	$[0, -4\sqrt{\frac{2}{3}}]$	$[0, \frac{4}{\sqrt{3}}]$	$\Xi_c\bar{D}^*$		$[-\frac{10}{3}, 0]$	$[0, -2]$	$[0, \frac{-2}{\sqrt{3}}]$	$[0, 2\sqrt{\frac{5}{3}}]$
$\Xi_c\bar{D}$			$[-\frac{10}{3}, 0]$	$[0, 0]$	$[0, 0]$	$[0, 2]$	$[0, 2\sqrt{2}]$	$\Xi_c^*\bar{D}$			$[-\frac{10}{3}, 0]$	$[0, -\frac{10}{3\sqrt{3}}]$	$[0, -\frac{10\sqrt{\frac{5}{3}}}{3}]$
$\Xi_c\bar{D}^*$				$[-\frac{10}{3}, 0]$	$[0, 2]$	$[0, -\frac{4}{\sqrt{3}}]$	$[0, 2\sqrt{\frac{2}{3}}]$	$\Xi_c'\bar{D}^*$				$[-\frac{10}{3}, -\frac{20}{9}]$	$[0, \frac{10\sqrt{5}}{9}]$
$\Xi_c'\bar{D}$					$[-\frac{10}{3}, 0]$	$[0, -\frac{20}{3\sqrt{3}}]$	$[0, \frac{10\sqrt{\frac{2}{3}}}{3}]$	$\Xi_c^*\bar{D}^*$					$[-\frac{10}{3}, \frac{20}{9}]$
$\Xi_c'\bar{D}^*$						$[-\frac{10}{3}, \frac{40}{9}]$	$[0, \frac{10\sqrt{2}}{9}]$						
$\Xi_c^*\bar{D}^*$							$[-\frac{10}{3}, \frac{50}{9}]$						

respectively. For example, the explicit form of the effective potential matrix for the $J = 3/2$ P_ψ^N states is

$$\mathbb{V}_{3/2}^{P_\psi^N} = \begin{pmatrix} \frac{2}{3}\tilde{g}_s & -2\sqrt{3}\tilde{g}_a & 2\tilde{g}_a & 2\sqrt{5}\tilde{g}_a \\ -2\sqrt{3}\tilde{g}_a & -\frac{10}{3}\tilde{g}_s & -\frac{10}{3\sqrt{3}}\tilde{g}_a & -\frac{10\sqrt{\frac{5}{3}}}{3}\tilde{g}_a \\ 2\tilde{g}_a & -\frac{10}{3\sqrt{3}}\tilde{g}_a & -\frac{10}{3}\tilde{g}_s - \frac{20}{9}\tilde{g}_a & \frac{10\sqrt{5}}{9}\tilde{g}_a \\ 2\sqrt{5}\tilde{g}_a & -\frac{10\sqrt{\frac{5}{3}}}{3}\tilde{g}_a & \frac{10\sqrt{5}}{9}\tilde{g}_a & -\frac{10}{3}\tilde{g}_s + \frac{20}{9}\tilde{g}_a \end{pmatrix}. \tag{17}$$

Similarly, the effective potential matrices $\mathbb{V}_{1/2}^{P_c}$, $\mathbb{V}_{1/2}^{P_{cs}}$, and $\mathbb{V}_{3/2}^{P_{cs}}$ can also be obtained directly from Tables II and III.

We use the masses of the observed P_ψ^N states as input to determine the coupling constants $\tilde{g}_s$ and $\tilde{g}_a$. In our previous work, we find that the Lagrangian in Eq. (7) can give a satisfactory description of the observed T_{cc} [40,41], P_ψ^N, and $P_{\psi s}^\Lambda$ states if we assign $P_\psi^N(4440)^+$ and $P_\psi^N(4457)^+$ as the $I(J^P) = 1/2(1/2^-)$ and $1/2(3/2^-)$ states. For consistency, we still adopt this set of assignments and use the masses of the $P_\psi^N(4440)^+$ and $P_\psi^N(4457)^+$ as inputs. In the coupled-channel formalism, the bound/quasibound states in the $J^P = 1/2^-$ and $3/2^-$ P_ψ^N systems satisfy the following equations:

$$\mathrm{Re}\|\mathbf{1} - \mathbb{V}_{1/2}^{P_\psi^N}\mathbb{G}_{1/2}^{P_\psi^N}\| = 0, \tag{18}$$

$$\mathrm{Im}\|\mathbf{1} - \mathbb{V}_{1/2}^{P_\psi^N}\mathbb{G}_{1/2}^{P_\psi^N}\| = 0, \tag{19}$$

$$\mathrm{Re}\|\mathbf{1} - \mathbb{V}_{3/2}^{P_\psi^N}\mathbb{G}_{3/2}^{P_\psi^N}\| = 0, \tag{20}$$

$$\mathrm{Im}\|\mathbf{1} - \mathbb{V}_{3/2}^{P_\psi^N}\mathbb{G}_{3/2}^{P_\psi^N}\| = 0. \tag{21}$$

These four equations can be solved numerically, and we get

$$\tilde{g}_s = 8.28\ \mathrm{GeV}^{-2}, \qquad \tilde{g}_a = -1.46\ \mathrm{GeV}^{-2}. \tag{22}$$

The imaginary parts of the pole positions of $P_\psi^N(4440)^+$ and $P_\psi^N(4457)^+$ can also be obtained from Eqs. (18)–(21).

B. Discussion on the form factor

In Ref. [33], we adopt a step function in the effective potential to exclude the contributions from higher momenta:

$$V(p,p') = V_{[BM]^I_J}\Theta(\Lambda - p)\Theta(\Lambda - p'). \quad (23)$$

For the bound state, the Green's function can be obtained analytically and have the expression

$$G = \frac{m_\mu}{\pi^2}\left[-\Lambda + q\tan^{-1}\left(\frac{\Lambda}{q}\right)\right], \qquad q = \sqrt{-2m_\mu E}. \quad (24)$$

Here, the $\tan^{-1}(\frac{\Lambda}{q})$ function has a singularity at $q = \Lambda$. In Ref. [33], we precisely solve the $\tilde{g}_s$, $\tilde{g}_a$, and Λ cases from three single-channel equations with the masses of $P_\psi^N(4312)$, $P_\psi^N(4440)$, and $P_\psi^N(4457)$ as inputs. We obtain $\Lambda = 0.409$ GeV. In the single-channel case, the discussed molecular candidates are very close to their corresponding thresholds. Thus, the condition $q \ll \Lambda$ is satisfied. However, in the multichannel case, if the two thresholds have a large mass gap, then $q \approx \Lambda$ is possible, which leads to a singularity at $q = \Lambda$. This singularity will appear like a "bound state" solution in the first Riemann sheet. Such a solution is artificially introduced by choosing the step function as the regulator. And it is difficult to distinguish these fake solutions from physical solutions, especially for our multichannel calculation. To avoid this difficulty, we introduce the dipole form factor $u(\Lambda) = (1 + q^2/\Lambda^2)^{-2}$.

In Ref. [33], Λ, $\tilde{g}_s$, and $\tilde{g}_a$ are precisely solved from three single-channel equations. In this work, we want to take into account the coupled-channel effect to determine our coupling parameters, and it is more complicated to numerically solve the coupled-channel equations with Λ, $\tilde{g}_s$, and $\tilde{g}_a$ as three undetermined parameters. To simplify our calculation, we fix Λ at 1.0 GeV, which is widely adopted in other literature [37,38], and select the $J^P = 1/2^-$ $P_\psi^N(4440)$ and $J^P = 3/2^-$ $P_\psi^N(4457)$ states as the inputs of Eqs. (18)–(21), respectively, to determine $\tilde{g}_s$ and $\tilde{g}_a$. Of course, we can set Λ to other values near 1.0 GeV; in that case, we obtain another set of $\tilde{g}_s$ and $\tilde{g}_a$ with $P_\psi^N(4440)$ and $P_\psi^N(4457)$ as inputs. But we find that the obtained masses of bound states only have weak Λ dependences.

In addition, if we refer to the procedures by which we determine the parameters Λ, $\tilde{g}_s$, and $\tilde{g}_a$ in Ref. [33] and in this work as Scheme 1 and Scheme 2, respectively, we can further perform a brief single-channel calculation on the masses of the states listed in Table III of Ref. [33]; the results are presented in Table IV. From Table IV, we find that the results obtained from the dipole form factor adopted in this work are still consistent with those in our previous work [33].

TABLE IV. The masses and binding energies of the molecular candidates considered in Table III of Ref. [33]. A step function $[\Theta(\Lambda - q)]$ [33] and a dipole form factor $[(1 + q^2/\Lambda^2)^{-2}]$ are introduced to regularize the integral in Scheme 1 and Scheme 2. The listed values are all in units of MeV.

	Scheme 1		Scheme 2	
	Mass [33]	BE [33]	Mass	BE
$T_{cc}(3875)^+$	3874.5	−1.8	3875.5	−0.8
$P_\psi^N(4312)^+$	4311.9	−8.9	4312.7	−8.7
$P_\psi^N(4380)^+$	4376.2	−9.1	4376.9	−8.5
$P_\psi^N(4440)^+$	4440.2	−21.8	4438.9	−23.2
$P_\psi^N(4457)^+$	4457.3	−4.8	4457.5	−4.6
$P_{\psi s}^\Lambda(4459)^0$	4468.1	−10.0	4468.3	−9.7

C. Flavor-spin symmetry of the P_ψ^N and $P_{\psi s}^\Lambda$ systems in the single-channel formalism

With the determined parameters $\tilde{g}_s$ and $\tilde{g}_a$, we first present our single-channel results for the considered P_ψ^N and $P_{\psi s}^\Lambda$ systems and demonstrate that we can relate the P_ψ^N and $P_{\psi s}^\Lambda$ systems from their interactions constrained by the SU(3) and heavy quark symmetries.

Although $\Xi_c\bar{D}$ and $\Sigma_c\bar{D}$ belong to different multiplets, in Ref. [31] we proposed that there exists a generalized flavor-spin symmetry between two-body heavy-flavor systems. For two different heavy-flavor meson-baryon systems, if they both possess the same flavor ($\langle H_1^f H_2^f|\boldsymbol{\lambda}_1\cdot\boldsymbol{\lambda}_2|H_1^f H_2^f\rangle$) and spin ($\langle H_1^s H_2^s|\boldsymbol{\sigma}_1\cdot\boldsymbol{\sigma}_2|H_1^s H_2^s\rangle$) matrix elements, they will still have identical effective potentials in the SU(3) and heavy quark limits.

In the single-channel formalism, we present the masses and binding energies of the P_ψ^N and $P_{\psi s}^\Lambda$ states in Table V. The theoretical uncertainties are introduced by considering the experimental errors of the masses of $P_\psi^N(4440)^+$ and $P_\psi^N(4457)^+$. We collect the P_ψ^N and $P_{\psi s}^\Lambda$ states that share identical effective potentials in the same row. As listed in Table V, the P_ψ^N and $P_{\psi s}^\Lambda$ states have similar binding energies in the same row and can be related via a flavor-spin symmetry.

D. The masses of P_ψ^N states in the multichannel formalism

Next, we explore how the coupled-channel effect influences the masses of the P_ψ^N states. As can be seen from Eq. (8), the effective potential consists of two parts—i.e., the central term ($\tilde{g}_s\boldsymbol{\lambda}_1\cdot\boldsymbol{\lambda}_2$) and the spin-spin interaction ($\tilde{g}_a\boldsymbol{\lambda}_1\cdot\boldsymbol{\lambda}_2\boldsymbol{\sigma}_1\cdot\boldsymbol{\sigma}_2$) term. Since the determined $\tilde{g}_s$ is much larger than $\tilde{g}_a$, the central term dominates the total effective potential and therefore determines whether the considered system can form a bound state.

As given in Table II, for the matrix elements in the P_ψ^N system, all the diagonal matrix elements have central terms,

TABLE V. In the single-channel formalism, the binding energies of the P_ψ^N and $P_{\psi s}^\Lambda$ states that share the same effective potentials in the SU(3) and heavy quark limits. All results are in units of MeV.

P_ψ^N	Mass	BE	$P_{\psi s}^\Lambda$	Mass	BE	V
$[\Sigma_c\bar{D}]^{\frac{1}{2}}$	$4312.7^{+4.1}_{-2.6}$	$-8.1^{+4.1}_{-2.6}$	$[\Xi_c\bar{D}]^{\frac{1}{2}}$	$4328.5^{+4.1}_{-2.7}$	$-8.2^{+4.1}_{-2.7}$	$-\frac{10}{3}\tilde{g}_s$
			$[\Xi_c\bar{D}^*]^{\frac{1}{2},\frac{3}{2}}$	$4468.3^{+4.5}_{-2.9}$	$-9.7^{+4.5}_{-2.9}$	
$[\Sigma_c^*\bar{D}]^{\frac{3}{2}}$	$4376.9^{+4.2}_{-2.7}$	$-8.5^{+4.2}_{-2.7}$	$[\Xi_c'\bar{D}]^{\frac{1}{2}}$	$4437.2^{+4.5}_{-2.8}$	$-8.8^{+4.3}_{-2.8}$	
			$[\Xi_c^*\bar{D}]^{\frac{3}{2}}$	$4503.9^{+4.4}_{-2.8}$	$-9.3^{+4.4}_{-2.8}$	
$[\Sigma_c\bar{D}^*]^{\frac{1}{2}}$	$4438.9^{+4.9}_{-8.9}$	$-23.2^{+4.9}_{-8.9}$	$[\Xi_c'\bar{D}^*]^{\frac{1}{2}}$	$4562.9^{+2.8}_{-9.1}$	$-24.5^{+2.8}_{-9.1}$	$-\frac{10}{3}\tilde{g}_s+\frac{40}{9}\tilde{g}_a$
$[\Sigma_c\bar{D}^*]^{\frac{3}{2}}$	$4457.5^{+3.7}_{-1.8}$	$-4.6^{+3.7}_{-1.8}$	$[\Xi_c'\bar{D}^*]^{\frac{3}{2}}$	$4582.2^{+4.0}_{-2.0}$	$-5.2^{+4.0}_{-2.0}$	$-\frac{10}{3}\tilde{g}_s-\frac{20}{9}\tilde{g}_a$
$[\Sigma_c^*\bar{D}^*]^{\frac{1}{2}}$	$4498.8^{+6.6}_{-6.0}$	$-27.9^{+6.6}_{-6.0}$	$[\Xi_c^*\bar{D}^*]^{\frac{1}{2}}$	$4625.3^{+6.8}_{-12.7}$	$-29.2^{+6.8}_{-12.7}$	$-\frac{10}{3}\tilde{g}_s+\frac{50}{9}\tilde{g}_a$
$[\Sigma_c^*\bar{D}^*]^{\frac{3}{2}}$	$4510.3^{+4.1}_{-4.1}$	$-16.4^{+4.1}_{-4.1}$	$[\Xi_c^*\bar{D}^*]^{\frac{3}{2}}$	$4637.9^{+4.3}_{-4.2}$	$-16.6^{+4.3}_{-4.2}$	$-\frac{10}{3}\tilde{g}_s+\frac{20}{9}\tilde{g}_a$

and some of them have corrections from the spin-spin interaction terms. The off-diagonal terms only consist of the spin-spin interaction terms. Thus, before we perform a practical multichannel calculation of the P_ψ^N system, we may anticipate that the coupled-channel effect would have small corrections to the masses of the P_ψ^N states.

As discussed in Sec. II, we include five and four channels to study the $J=1/2$ and $J=3/2$ P_ψ^N states, respectively. For the $J=1/2$ channels, according to their thresholds, we consider five energy regions:

$$E \le m_{\Lambda_c\bar{D}}, \tag{25}$$

$$m_{\Lambda_c\bar{D}} < E \le m_{\Lambda_c\bar{D}^*}, \tag{26}$$

$$m_{\Lambda_c\bar{D}^*} < E \le m_{\Sigma_c\bar{D}}, \tag{27}$$

$$m_{\Sigma_c\bar{D}} < E \le m_{\Sigma_c\bar{D}^*}, \tag{28}$$

$$m_{\Sigma_c\bar{D}^*} < E \le m_{\Sigma_c^*\bar{D}^*}. \tag{29}$$

We search the bound (quasibound)-state solutions below the higher threshold in each energy region on the first Riemann sheet. The bound (quasibound)-state solutions of the $J=3/2$ P_ψ^N, $J=1/2$, and $3/2$ $P_{\psi s}^\Lambda$ states can be found by repeating the same procedure. We present the obtained P_ψ^N states in Table VI. We do not find any bound states below the $\Lambda_c\bar{D}$ threshold. Thus, all the obtained resonances (E_R) listed in Table VI should refer to quasibound states and have imaginary parts [$\mathrm{Im}(E_R)$]. Since we only include the two-body open-charm decay channels, the estimated widths (Γ) in Table VI are smaller than experimental widths. By comparing the masses of P_ψ^N states in Tables V and VI, we find that the coupled-channel effect indeed has a small influence on the masses of the P_ψ^N states.

E. A numerical experiment on the ($\Lambda_c\bar{D}_s^{(*)}$, $\Xi_c\bar{D}^{(*)}$) coupled-channel systems

There exists an important difference between the effective potential matrices in the P_ψ^N and $P_{\psi s}^\Lambda$ systems. As presented in Tables II and III, the diagonal matrix elements in the $P_{\psi s}^\Lambda$ system are very similar to those of the P_ψ^N system. But for the off-diagonal matrix elements, the effective potentials of the $\Lambda_c\bar{D}_s-\Xi_c\bar{D}$ and $\Lambda_c\bar{D}_s^*-\Xi_c\bar{D}^*$ channels in the $P_{\psi s}^\Lambda$ system with $J=1/2$ or $3/2$ consist of central terms. These terms may give considerable corrections to the spectrum of the $P_{\psi s}^\Lambda$ states.

For the $J=1/2$ and $J=3/2$ $P_{\psi s}^\Lambda$ systems, as given in Eqs. (5) and (6), we need to perform seven and five

TABLE VI. The results of P_ψ^N states obtained in the coupled-channel formalism. Here, $\Gamma=-2\mathrm{Im}(E_R)$, and all the results are in units of MeV.

		Our		Exp	
State	J^P	Mass	Γ	Mass	Width
$P_\psi^N(4312)^+$	$\frac{1}{2}^-$	$4308.2^{+2.6}_{-4.5}$	$2.6^{+2.4}_{-1.7}$	$4311.9^{+7.0}_{-0.9}$	10 ± 5
$P_\psi^N(4440)^+$	$\frac{1}{2}^-$	$4440.3^{+4.0}_{-5.0}$ (input)	$9.8^{+4.6}_{-5.8}$	$4440.3^{+4.0}_{-5.0}$	21^{+10}_{-11}
$P_\psi^N(4457)^+$	$\frac{3}{2}^-$	$4457.7^{+4.0}_{-1.8}$ (input)	$2.0^{+1.4}_{-0.8}$	$4457.3^{+4.0}_{-1.8}$	$6.4^{+6.0}_{-2.8}$
$P_\psi^N(4380)$	$\frac{3}{2}^-$	$4373.3^{+3.4}_{-6.8}$	$5.2^{+20.2}_{-3.5}$	...	...
$P_\psi^N(4500)$	$\frac{1}{2}^-$	$4501.4^{+5.0}_{-6.2}$	$8.8^{+17.2}_{-5.4}$	...	...
$P_\psi^N(4510)$	$\frac{3}{2}^-$	$4513.4^{+5.8}_{-3.1}$	$7.6^{+9.4}_{-0.0}$	...	...

coupled-channel calculations, respectively. Before we perform such complete calculations, we first perform a detailed discussion on the ($\Lambda_c\bar{D}_s$, $\Xi_c\bar{D}$) and ($\Lambda_c\bar{D}_s^*$, $\Xi_c\bar{D}^*$) coupled-channel systems.

The effective potential matrixes of the $J=1/2$ ($\Lambda_c\bar{D}_s$, $\Xi_c\bar{D}$), ($\Lambda_c\bar{D}_s^*$, $\Xi_c\bar{D}^*$) systems and the $J=3/2$ ($\Lambda_c\bar{D}_s^*$, $\Xi_c\bar{D}^*$) system share the same expressions in the heavy quark limit. From Table III, we obtain the corresponding effective potential matrix,

$$\mathbb{V}=\begin{pmatrix} v_{11} & v_{12} \\ v_{21} & v_{22} \end{pmatrix}, \tag{30}$$

with

$$v_{11}=-\frac{4}{3}\tilde{g}_s, \qquad v_{22}=-\frac{10}{3}\tilde{g}_s, \tag{31}$$

$$v_{12}=v_{21}=2\sqrt{2}\tilde{g}_s g_x. \tag{32}$$

Here, for the diagonal matrix elements listed in Tables II and III, their dominant components are from the exchange of the nonstrange light scalar meson currents. Since the interactions of the off-diagonal channel $\Lambda_c\bar{D}_s^{(*)}-\Xi_c\bar{D}^{(*)}$ are introduced via the exchange of the strange scalar meson currents, we further introduce a factor g_x to estimate the SU(3) breaking effects. Compared with the exchange of the nonstrange light scalar meson currents, the off-diagonal matrix elements should be suppressed by the mass of strange mesons. Thus, we assume $0\le gx\le 1$. This factor also reflects the coupling strength of the $\Lambda_c\bar{D}_s-\Xi_c\bar{D}$ channel. With $g_x=0$, the $\Lambda_c\bar{D}_s^{(*)}$ does not couple to the $\Xi_c\bar{D}^{(*)}$ channel. With $g_x=1.0$, the $\Lambda_c\bar{D}_s^{(*)}$ couples to the $\Xi_c\bar{D}^{(*)}$ channel, and its coupling strength is set to be the value in the SU(3) limit.

In Fig. 1(b), we present the variation of the masses for the bound states $P_{\psi s}^{\Lambda}(4338)^0$ and $P_{\psi s}^{\Lambda}(4255)^0$ as the parameter g_x increases. The masses of $P_{\psi s}^{\Lambda}(4338)^0$ and $P_{\psi s}^{\Lambda}(4255)^0$ are denoted with black lines. At $g_x=0$, the $\Lambda_c\bar{D}_s$ channel itself has a weak attractive force $v_{11}=-4/3\tilde{g}_s$, and this force is too weak to form a $\Lambda_c\bar{D}_s$ bound state. On the contrary, the $\Xi_c\bar{D}$ channel can form a bound state, and its mass is about $M=4329$ MeV, slightly smaller than the experimental value. As g_x increases, the attractive force of $P_{\psi s}^{\Lambda}(4338)^0$ decreases, and its mass moves closer to the $\Xi_c\bar{D}$ threshold. In a very narrow region $0.62\le g_x\le 0.64$, the attractive force is just enough to form a $P_{\psi s}^{\Lambda}(4338)^0$ bound state at the $\Xi_c\bar{D}$ threshold, and the weak attractive channel $\Lambda_c\bar{D}_s$ starts to form a bound state due to the $\Xi_c\bar{D}-\Lambda_c\bar{D}_s$ coupling. Only in this very narrow region can $P_{\psi s}^{\Lambda}(4338)^0$ and $P_{\psi s}^{\Lambda}(4255)^0$ coexist as quasibound states. At $g_x>0.64$, the $\Xi_c\bar{D}-\Lambda_c\bar{D}_s$ coupling further weakens the attractive force of the $\Xi_c\bar{D}$ channel and $P_{\psi s}^{\Lambda}(4338)^0$ no longer exists as a quasibound state, while the attractive force of the $\Lambda_c\bar{D}_s$ channel becomes stronger, and its mass will decrease. The observation of the $P_{\psi s}^{\Lambda}(4338)^0$ by LHCb seems to exclude the parameter region $0.64<g_x<1.0$.

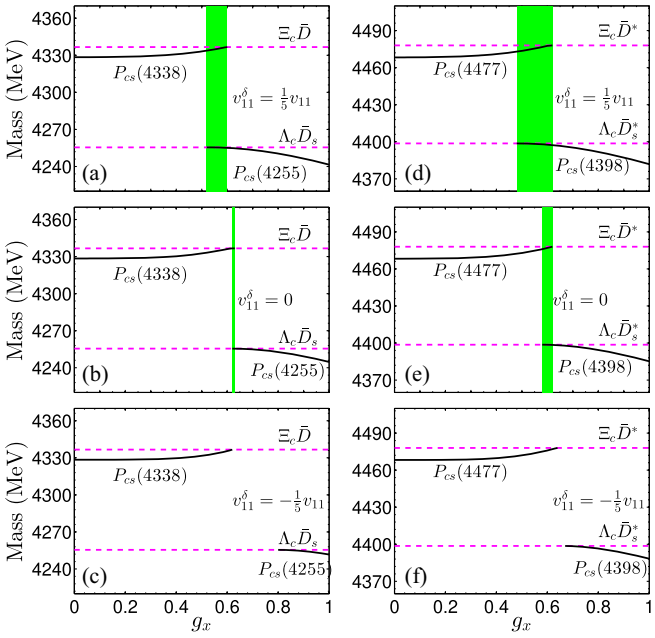

FIG. 1. The variations of the masses for the possible bound states in the ($\Lambda_c\bar{D}_s^{(*)}$ $\Xi_c\bar{D}^{(*)}$) two-channel system as the parameter g_x increases. We use the blue dotted lines to denote the $\Lambda_c\bar{D}_s^{(*)}$ and $\Xi_c\bar{D}^{(*)}$ thresholds. The masses of the $P_{\psi s}^{\Lambda}$ states are denoted with black lines. Panels (a), (d), panels (b), (e), and panels (c), (f) are obtained at $v_{11}^\delta=1/5v_{11}$, 0, and $-1/5v_{11}$, respectively. The green bands in (a), (d), (b), and (e) denote that the bound states near the $\Lambda_c\bar{D}_s$ ($\Lambda_c\bar{D}_s^*$) and $\Xi_c\bar{D}$ ($\Xi_c\bar{D}^*$) thresholds can coexist in this g_x region.

Here, we also check the pole position of $P_{\psi s}^{\Lambda}(4338)^0$ at $g_x>0.64$ in the energy region slightly above the $\Xi_c\bar{D}$ threshold. We find that the pole of $P_{\psi s}^{\Lambda}(4338)^0$ still exists in the first Riemann sheet. This is mainly due to the fact that the $\Lambda_c\bar{D}_s-\Xi_c\bar{D}$ coupling leads $P_{\psi s}^{\Lambda}(4338)^0$ to be a state that has a considerable width; thus, the central value of the $P_{\psi s}^{\Lambda}(4338)^0$ mass may cross the $\Xi_c\bar{D}$ threshold. In this case, $P_{\psi s}^{\Lambda}(4338)^0$ should be interpreted as a quasibound state above the $\Xi_c\bar{D}$ threshold. Nevertheless, in this work, we restrict our scope to the case in which the masses of the bound/quasibound states are below their corresponding thresholds.

To understand why the g_x region that allows the $P_{\psi s}^{\Lambda}(4338)^0$ and $P_{\psi s}^{\Lambda}(4255)^0$ states to coexist is so narrow, we further check the role of the $\Lambda_c\bar{D}_s$ channel in our two-channel model. We allow the effective potential of the $\Lambda_c\bar{D}_s$ channel to have a 20% shift—i.e.,

$$v_{11}'=v_{11}+v_{11}^\delta, \qquad v_{11}^\delta=0,\pm\frac{1}{5}v_{11}, \tag{33}$$

and we further check how the masses of $P^{\Lambda}_{\psi s}(4338)^0$ and $P^{\Lambda}_{\psi s}(4255)^0$ change as we increase the value of g_x.

The channel $\Lambda_c\bar{D}_s$ itself has a weak attractive force, as presented in Fig. 1(a), at $g_x = 0$. After we increase this force by 20%, this single channel still cannot form a bound state. But the g_x region that allows these two $P^{\Lambda}_{\psi s}$ states to coexist becomes broader. On the contrary, as illustrated in Fig. 1(c), if we decrease the attractive force of the $\Lambda_c\bar{D}_s$ channel by 20%, then $P^{\Lambda}_{\psi s}(4338)^0$ and $P^{\Lambda}_{\psi s}(4255)^0$ cannot coexist, no matter how we adjust the off-diagonal $\Lambda_c\bar{D}_s - \Xi_c\bar{D}$ coupling. Thus, the narrow g_x region within which $P^{\Lambda}_{\psi s}(4338)^0$ and $P^{\Lambda}_{\psi s}(4255)^0$ can coexist is due to the fact that the $\Lambda_c\bar{D}_s$ channel has a small but non-negligible attractive force.

The results for the $J = 1/2$ and $3/2$ ($\Lambda_c\bar{D}^*_s$,$\Xi_c\bar{D}^*$) coupled channels are presented in Figs. 1(d)–1(f). We find that the roles of the predicted $P^{\Lambda}_{\psi s}(4477)^0$ and $P^{\Lambda}_{\psi s}(4398)^0$ with $J^P = 1/2^-$ or $3/2^-$ are very similar to those of the $P^{\Lambda}_{\psi s}(4338)^0$ and $P^{\Lambda}_{\psi s}(4255)^0$ with $J^P = 1/2^-$, respectively.

F. The results of $P^{\Lambda}_{\psi s}$ system in the coupled-channel formalism

We present our complete multichannel calculations on the $J = 1/2$ and $J = 3/2$ $P^{\Lambda}_{\psi s}$ systems in Fig. 2. We find that only the bound states close to the $\Lambda_c\bar{D}^{(*)}_s$ and $\Xi_c\bar{D}^{(*)}$ channels have a significant dependence on g_x, since these bound states can couple to the $\Lambda_c\bar{D}^{(*)}_s$ and $\Xi_c\bar{D}^{(*)}$ channels through non-negligible central terms, while the bound states that can only couple to the $\Lambda_c\bar{D}^{(*)}_s$ and $\Xi_c\bar{D}^{(*)}$ channels via the spin-spin interaction terms have a very tiny dependence on the parameter g_x.

To further present our numerical results, we fix the parameter g_x at 0.5 and at 0.62. We denote these two cases as case 1 and case 2. These cases correspond to the results when the possible $P^{\Lambda}_{\psi s}(4255)^0$ signal does not/does exist. The results of these two cases are listed in Table VII.

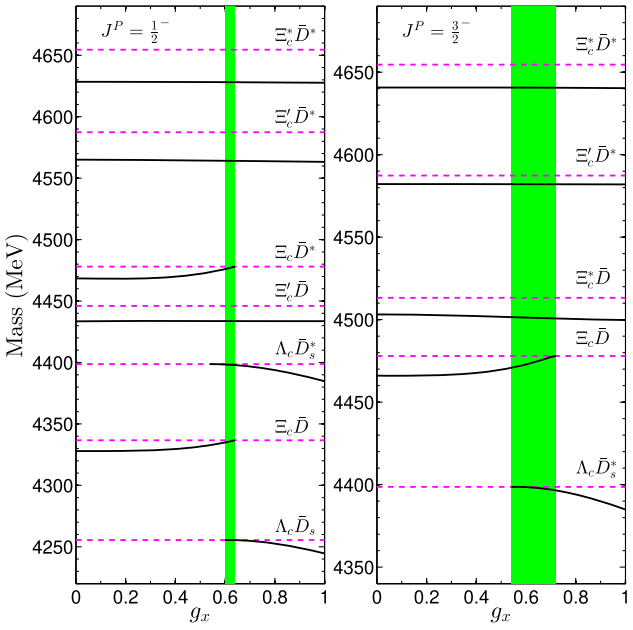

FIG. 2. The variations of the masses for the $P^{\Lambda}_{\psi s}$ states with $J^P = 1/2^-$ and $J^P = 3/2^-$ as g_x increases. We use blue dotted lines to denote the considered meson-baryon thresholds. The masses of the obtained bound states are denoted with black lines. The green bands denote that the bound states near the $\Lambda_c\bar{D}^{(*)}_s$ or $\Xi_c\bar{D}^{(*)}$ thresholds can coexist in this g_x region.

Comparing the masses of the $P^{\Lambda}_{\psi s}$ states calculated in the single-channel formalism (Table V) with the results obtained in the coupled-channel formalism (Table VII),

TABLE VII. The results of the $P^{\Lambda}_{\psi s}$ states calculated at $g_x = 0.50$ and $g_x = 0.62$ in the coupled-channel formalism. All results are in units of MeV.

	$g_x = 0.50$			$g_x = 0.62$		
States	Mass	Γ	BE	Mass	Γ	BE
$[\Lambda_c\bar{D}_s]^{\frac{1}{2}}$	⋯	⋯	⋯	$4255.5^{+0.0}_{-0.7}$	0.0	$-0.0^{+0.0}_{-0.7}$
$[\Lambda_c\bar{D}^*_s]^{\frac{1}{2}}$	⋯	⋯	⋯	$4398.1^{+0.2}_{-1.5}$	0.0	$-0.6^{+0.2}_{-1.5}$
$[\Lambda_c\bar{D}^*_s]^{\frac{3}{2}}$	⋯	⋯	⋯	$4398.3^{+0.4}_{-1.3}$	0.0	$-0.4^{+0.4}_{-1.3}$
$[\Xi_c\bar{D}]^{\frac{1}{2}}$	$4331.6^{+2.6}_{-1.5}$	$17.8^{+3.6}_{-7.6}$	$-5.0^{+2.6}_{-1.5}$	$4335.9^{+0.7}_{-2.1}$	$26.0^{+5.0}_{-10.2}$	$-0.7^{+0.7}_{-2.1}$
$[\Xi_c\bar{D}^*]^{\frac{1}{2}}$	$4472.1^{+2.5}_{-1.6}$	$23.4^{+5.2}_{-6.0}$	$-5.9^{+2.5}_{-1.6}$	$4477.1^{+0.5}_{-0.8}$	$33.0^{+6.0}_{-8.0}$	$-0.9^{+0.5}_{-0.8}$
$[\Xi_c\bar{D}^*]^{\frac{3}{2}}$	$4469.7^{+1.9}_{-6.6}$	$14.6^{+4.4}_{-10.6}$	$-8.3^{+1.9}_{-6.6}$	$4473.7^{+2.7}_{-8.7}$	$20.2^{+5.8}_{-13.6}$	$-4.7^{+2.7}_{-8.7}$
$[\Xi_c'\bar{D}]^{\frac{1}{2}}$	$4433.8^{+3.4}_{-4.8}$	$0.8^{+5.0}_{-0.6}$	$-12.2^{+3.4}_{-4.8}$	$4433.7^{+3.5}_{-5.2}$	$0.4^{+2.6}_{-0.0}$	$-12.3^{+3.5}_{-5.2}$
$[\Xi_c^*\bar{D}]^{\frac{3}{2}}$	$4501.8^{+4.4}_{-3.4}$	$7.7^{+22.3}_{-5.1}$	$-11.4^{+4.4}_{-3.4}$	$4501.2^{+4.2}_{-3.7}$	$7.8^{+25.4}_{-5.3}$	$-12.0^{+4.2}_{-3.7}$
$[\Xi_c'\bar{D}^*]^{\frac{1}{2}}$	$4564.4^{+3.4}_{-4.0}$	$4.5^{+9.5}_{-2.7}$	$-23.0^{+3.4}_{-4.0}$	$4564.1^{+3.3}_{-7.4}$	$4.8^{+9.2}_{-2.8}$	$-23.3^{+3.3}_{-7.4}$
$[\Xi_c'\bar{D}^*]^{\frac{3}{2}}$	$4582.1^{+4.3}_{-2.0}$	$1.9^{+0.7}_{-1.1}$	$-5.3^{+4.3}_{-2.0}$	$4582.1^{+4.2}_{-2.0}$	$2.0^{+1.3}_{-1.2}$	$-5.3^{+4.2}_{-2.0}$
$[\Xi_c^*\bar{D}^*]^{\frac{1}{2}}$	$4628.2^{+3.5}_{-7.1}$	$5.0^{+9.0}_{-3.0}$	$-26.3^{+3.5}_{-7.1}$	$4628.1^{+5.1}_{-7.3}$	$5.2^{+24.5}_{-3.2}$	$-26.4^{+5.1}_{-7.3}$
$[\Xi_c^*\bar{D}^*]^{\frac{3}{2}}$	$4640.7^{+5.8}_{-3.2}$	$7.0^{+8.2}_{-0.8}$	$-13.8^{+5.8}_{-3.2}$	$4640.6^{+5.9}_{-3.2}$	$7.2^{+8.4}_{-4.4}$	$-13.9^{+5.9}_{-3.2}$

we infer that the off-diagonal channels that only consist of the spin-spin interaction terms have a small influence on the masses of the $P_{\psi s}^{\Lambda}$ states, which is very similar to the P_ψ^N system. From Table VII, we find that there exist three extra $P_{\psi s}^{\Lambda}$ states below the $\Lambda_c\bar{D}_s^{(*)}$ thresholds in case 2.

For the $P_{\psi s}^{\Lambda}(4338)^0$ state, due to its strong coupling to the $\Lambda_c\bar{D}_s$ channel, the width of this state is broader than the result given by LHCb. Note that in our calculation, we only include the open-charm two-body meson-baryon channels. Thus, the width predicted by our model should be regarded as the lower limit of the experimental width. Since $P_{\psi s}^{\Lambda}(4338)^0$ is reported in the $B \to J/\Psi\Lambda\bar{p}$ channel, the narrow width of the $P_{\psi s}^{\Lambda}(4338)^0$ found by the LHCb may be due to the small phase space of this B-meson decay process. Thus, confirming $P_{\psi s}^{\Lambda}(4338)^0$ in other decay processes is important to pinning down its resonance parameters.

Besides, we also find that the $P_{\psi s}^{\Lambda}$ states that are close to the $\Xi_c\bar{D}^{(*)}$ states are broader than the other $P_{\psi s}^{\Lambda}$ states due to their strong coupling to the $\Lambda_c\bar{D}_s^{(*)}$ channel. Thus, our results suggest that there exist two $J^P = 1/2^-$ and $J^P = 3/2^-$ quasibound states near the $\Xi_c\bar{D}^*$ region. This region is close to the reported $P_{\psi s}^{\Lambda}(4459)^0$, and the two-peak structure in this region has been discussed in a great deal of the literature [5,9,14,42,43]. The results from our model provide a new possibility—i.e., the two $P_{\psi s}^{\Lambda}$ structures in this region may have a significant overlap in the $J/\Psi\Lambda$ invariant spectrum due to their considerable widths. The decay behaviors of $P_{\psi s}^{\Lambda}(4459)^0$ have been discussed in Refs. [12,30,44–46]. The decay widths and decay patterns are valuable in identifying the structure of the $P_{\psi s}^{\Lambda}(4459)^0$ state. Further investigations on the total and partial decay widths will be crucial to accomplishing a thorough understanding on the P_ψ^N and $P_{\psi s}^{\Lambda}$ states.

G. The correspondence between the P_ψ^N and $P_{\psi s}^{\Lambda}$ systems

Finally, we compare the masses of the P_ψ^N and $P_{\psi s}^{\Lambda}$ states obtained from our multichannel model. The mass of the constituent s quark is heavier than those of the u and d quarks by about 100 MeV. Thus, we shift the mass plot of the $P_{\psi s}^{\Lambda}$ system by 100 MeV to check the similarities between the P_ψ^N and $P_{\psi s}^{\Lambda}$ states. We present the multichannel results for the P_ψ^N system in Fig. 3(a), and the multichannel results for the $P_{\psi s}^{\Lambda}$ system calculated at $g_x = 0.5$ and $g_x = 0.62$ are given in Fig. 3(b). As can be seen from Figs. 3(a) and 3(b), the meson-baryon thresholds in the P_ψ^N and $P_{\psi s}^{\Lambda}$ systems have the following analogies:

$$m_{\Lambda_c\bar{D}^{(*)}} \leftrightarrow m_{\Lambda_c\bar{D}_s^{(*)}}, \tag{34}$$

$$m_{\Sigma_c^{(*)}\bar{D}^{(*)}} \leftrightarrow m_{\Xi_c^{\prime(*)}\bar{D}^{(*)}}. \tag{35}$$

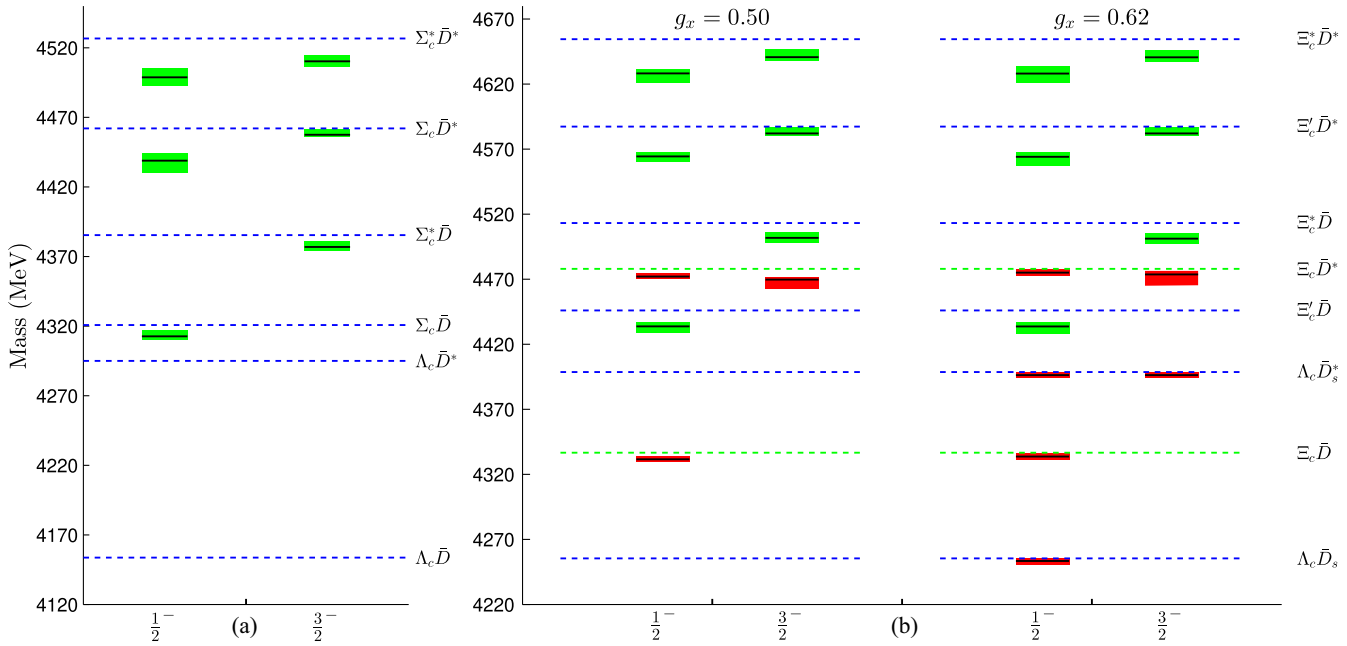

FIG. 3. The mass spectra of the P_ψ^N and $P_{\psi s}^{\Lambda}$ states in the multichannel formalism. We present the results of the $P_{\psi s}^{\Lambda}$ system at $g_x = 0.50$ and $g_x = 0.62$. The meson-baryon thresholds $m_{\Lambda_c\bar{D}^{(*)}}$, $m_{\Lambda_c\bar{D}_s^{(*)}}$, $m_{\Sigma_c^{(*)}\bar{D}^{(*)}}$, and $m_{\Xi_c^{\prime(*)}\bar{D}^{(*)}}$ are illustrated with blue dotted lines. The two extra thresholds, $\Xi_c\bar{D}$ and $\Xi_c\bar{D}^*$ in the $P_{\psi s}^{\Lambda}$, system are denoted with green dotted lines. We use black lines to denote the central values of the obtained P_ψ^N and $P_{\psi s}^{\Lambda}$ states, and their uncertainties are illustrated with green and red rectangles. The six green states in the P_ψ^N system can directly correspond to the six green states in the $P_{\psi s}^{\Lambda}$ system.

We denote these thresholds with blue dotted lines in Fig. 3. Besides these, there exist two extra meson-baryon thresholds, $\Xi_c\bar{D}$ and $\Xi_c\bar{D}^*$ in the $P^{\Lambda}_{\psi s}$ system. These two channels cannot directly correspond to the meson-baryon channels in the P^N_ψ system. We denote these two thresholds with green dotted lines.

As can be seen from Fig. 3, there exist six P^N_ψ states with $J^P = 1/2^-$ or $3/2^-$. These six states can correspond to the six states in the $P^{\Lambda}_{\psi s}$ system. We denote the masses of the central values of these 12 states with black lines, and their uncertainties are denoted with green rectangles. According to Fig. 3, the experimentally observed P^N_ψ states and the predicted $P^{\Lambda}_{\psi s}$ states should have the following analogies:

$$P^N_\psi(4312)^+ \leftrightarrow P^{\Lambda}_{\psi s}(4434)^0, \tag{36}$$

$$P^N_\psi(4440)^+ \leftrightarrow P^{\Lambda}_{\psi s}(4564)^0, \tag{37}$$

$$P^N_\psi(4457)^+ \leftrightarrow P^{\Lambda}_{\psi s}(4582)^0. \tag{38}$$

As indicated in Fig. 3, if we replace the $\Lambda_c\bar{D}_s^*$ and $\Xi_c'\bar{D}$ channels with the $\Xi_c\bar{D}$ and $\Xi_c\bar{D}^*$ channels, respectively, we can reluctantly obtain the following analogies:

$$P^N_\psi(4312)^+ \leftrightarrow P^{\Lambda}_{\psi s}(4472)^0, \tag{39}$$

$$P^N_\psi(4440)^+ \leftrightarrow P^{\Lambda}_{\psi s}(4564)^0, \tag{40}$$

$$P^N_\psi(4457)^+ \leftrightarrow P^{\Lambda}_{\psi s}(4582)^0. \tag{41}$$

The predicted $P^{\Lambda}_{\psi s}(4472)^0$ may correspond to the reported $P^{\Lambda}_{\psi s}(4459)^0$. However, such an analogy indicates a considerable SU(3)-breaking effect. In both sets of analogies, $P^{\Lambda}_{\psi s}(4338)^0$ cannot directly correspond to the lowest $P^N_\psi(4312)^+$ state.

There exist three and six extra $P^{\Lambda}_{\psi s}$ states that cannot correspond to the states in the P^N_ψ system at $g_x = 0.50$ and $g_x = 0.62$, respectively. We denote the masses of the central values of these states with black lines, and their uncertainties are denoted with red rectangles. Further experimental explorations on the $P^{\Lambda}_{\psi s}$ system may help us to distinguish which case should be preferred.

IV. SUMMARY

Motivated by the recently discovered $P^{\Lambda}_{\psi s}(4338)^0$ from the LHCb Collaboration, we have performed a multichannel calculation of the $I = 1/2$ P^N_ψ and $I = 0$ $P^{\Lambda}_{\psi s}$ systems and presented a comparison between the interactions of the P^N_ψ and $P^{\Lambda}_{\psi s}$ states in the $\mathrm{SU(3)_f}$ limit and heavy quark limit.

Unlike the $\bar{c}n - cnn$ $(n = u,\ d)$-type meson-baryon channels in the P^N_ψ system, we need to consider two types of channels when we study the $P^{\Lambda}_{\psi s}$ system—i.e., the $\bar{c}n - cns$ and $\bar{c}s - cnn$ meson-baryon channels. This difference will lead to extra states in the $P^{\Lambda}_{\psi s}$ systems.

The effective potentials of the P^N_ψ and $P^{\Lambda}_{\psi s}$ states are collectively obtained via a quark-level Lagrangian, which allows us to construct the correspondence between the P^N_ψ and $P^{\Lambda}_{\psi s}$ systems.

We use the masses of $P^N_\psi(4440)^+$ and $P^N_\psi(4457)^+$ as input to determine the coupling parameters $\tilde{g}_s$ and $\tilde{g}_a$ in our model. We first study the masses of the P^N_ψ states in the single-channel and coupled-channel formalisms. Since all the off-diagonal terms in the effective potential matrices consist of the spin-spin interaction terms, the coupled-channel effect provides very small corrections to the masses of the P^N_ψ states.

There exists an important difference between the P^N_ψ system and $P^{\Lambda}_{\psi s}$ system. In the $P^{\Lambda}_{\psi s}$ system, the off-diagonal terms $\Lambda_c\bar{D}_s^{(*)} - \Xi_c\bar{D}^{(*)}$ in the effective potential matrices consist of the central terms and will have considerable corrections to the mass spectrum of the $P^{\Lambda}_{\psi s}$ states. To clarify the role of the $\Lambda_c\bar{D}_s^{(*)} - \Xi_c\bar{D}^{(*)}$ coupling, we have performed a numerical experiment on the $(\Lambda_c\bar{D}_s^{(*)}, \Xi_c\bar{D}^{(*)})$ coupled-channel system. Our results suggest that the mass of the $P^{\Lambda}_{\psi s}(4338)^0$ may shift very close to the $\Xi_c\bar{D}$ threshold by adjusting the coupling between the $\Xi_c\bar{D}$ and $\Lambda_c\bar{D}_s$ channels. This coupling may also lead to a $P^{\Lambda}_{\psi s}(4255)^0$ state in a reasonable g_x region.

Then we present our complete multichannel calculations of the $P^{\Lambda}_{\psi s}$ systems. Since the $P^{\Lambda}_{\psi s}(4255)^0$ is not confirmed by experiment, we present our numerical results with $g_x = 0.50/0.62$, corresponding to the case in which the $P^{\Lambda}_{\psi s}(4255)^0$ does not/does exist, respectively. Due to the strong $\Lambda_c\bar{D}_s - \Xi_c\bar{D}$ couplings, our predicted width of $P^{\Lambda}_{\psi s}(4338)^0$ is broader than the experimental value. The reported narrower width may be due to the small phase space of the B-meson decay process. Confirming the $P^{\Lambda}_{\psi s}(4338)^0$ state in other processes will be helpful to pin down its resonance parameters. There exist two $P^{\Lambda}_{\psi s}$ states with $J^P = 1/2^-$ and $J^P = 3/2^-$ below the $\Xi_c\bar{D}^*$ threshold. The masses of these two states are close to the mass of the reported $P^{\Lambda}_{\psi s}(4459)^0$. Due to the $\Lambda_c\bar{D}_s^* - \Xi_c\bar{D}^*$ coupling, these two states should have considerable widths and may have significant overlap in the $J/\Psi\Lambda$ invariant spectrum. Further experimental exploration would be important to test our predictions.

Finally, we present a complete correspondence between the P^N_ψ and $P^{\Lambda}_{\psi s}$ states. The observed $P^N_\psi(4312)^+$, $P^N_\psi(4440)^+$, and $P^N_\psi(4457)^+$ do not directly correspond to the observed $P^{\Lambda}_{\psi s}(4338)^0$ and $P^{\Lambda}_{\psi s}(4459)^0$. It is particularly interesting to find the SU(3) $P^{\Lambda}_{\psi s}$ states that may correspond to the observed P^N_ψ states, and to investigate if such a correspondence does exist. Further experimental

researches on these topics will be helpful to fulfill a complete picture on the spectra of the P_ψ^N and $P_{\psi s}^\Lambda$ systems.

ACKNOWLEDGMENTS

This research is supported by the National Science Foundation of China under Grants No. 11975033, No. 12070131001, and No. 12147168.

APPENDIX: FLAVOR AND SPIN WAVE FUNCTIONS FOR THE CONSIDERED MESON-BARYON SYSTEMS

Similarly to the one-boson-exchange model or resonance saturation model, in our framework, a meson and a baryon can interact with each other via exchanging light mesons, but we describe such a process with a quark-level Lagrangian. Thus, the flavor and spin wave functions are constructed at the hadron level, and we further rephrase them into quark-level forms. In Tables VIII and IX, we present the flavor and spin wave functions of charmed hadrons we used in this work.

With the flavor and spin bases presented in Tables VIII and IX, we can construct the total quark-level flavor-spin wave function of a specific $[BM]^{II_z}_{JJ_z}$ system according to Eq. (11). For example, the explicit forms of the total wave functions of the $[\Sigma_c\bar{D}]^{\frac{11}{22}}_{\frac{11}{22}}$ and $[\Xi_c\bar{D}]^{00}_{\frac{11}{22}}$ systems can be directly obtained as

$$\left|[\Sigma_c\bar{D}]^{\frac{11}{22}}_{\frac{11}{22}}\right\rangle = \left[\sqrt{\frac{2}{3}}uucd\bar{c} - \sqrt{\frac{1}{6}}(udc+duc)u\bar{c}\right] \otimes \left[\sqrt{\frac{1}{3}}\uparrow\uparrow\downarrow(\uparrow\downarrow-\downarrow\uparrow) - \sqrt{\frac{1}{12}}(\uparrow\downarrow\uparrow+\downarrow\uparrow\uparrow)(\uparrow\downarrow-\downarrow\uparrow)\right], \tag{A1}$$

$$\left|[\Xi_c\bar{D}]^{00}_{\frac{11}{22}}\right\rangle = \left[\frac{1}{2}(usc-suc)d\bar{c} - \frac{1}{2}(dsc-sdc)u\bar{c}\right] \otimes \left[\frac{1}{2}(\uparrow\downarrow\uparrow-\downarrow\uparrow\uparrow)(\uparrow\downarrow-\downarrow\uparrow)\right]. \tag{A2}$$

We explicitly expand Eqs. (A1) and (A2) to calculate their corresponding $\langle\boldsymbol{\lambda}_1\cdot\boldsymbol{\lambda}_2\rangle$ and $\langle\boldsymbol{\lambda}_1\cdot\boldsymbol{\lambda}_2\boldsymbol{\sigma}_1\cdot\boldsymbol{\sigma}_2\rangle$ matrix elements.

The wave functions for the $[\Sigma_c\bar{D}]^{\frac{1}{2}}_{\frac{1}{2}}$ and $[\Xi_c\bar{D}]^{0}_{\frac{1}{2}}$ systems with other I_z and J_z components can be obtained in a similar way, and we can obtain the total wave functions of the rest of the considered baryon-meson systems by repeating the same procedure.

TABLE VIII. The flavor wave functions for the charmed hadrons considered in this work.

Hadron	$\lvert Im_I\rangle$	$\phi^{M_f}_{Im_I}$	Hadron	$\lvert Im_I\rangle$	$\phi^{M_f}_{Im_I}$
$\bar{D}^{(*)0}$	$\lvert\frac{1}{2}\frac{1}{2}\rangle$	$u\bar{c}$	$\bar{D}^{(*)-}$	$\lvert\frac{1}{2}-\frac{1}{2}\rangle$	$d\bar{c}$
$\bar{D}_s^{(*)-}$	$\lvert00\rangle$	$s\bar{c}$			
Hadron	$\lvert Im_I\rangle$	$\phi^{B_f}_{Im_I}$	Hadron	$\lvert Im_I\rangle$	$\phi^{B_f}_{Im_I}$
Λ_c^+	$\lvert00\rangle$	$\frac{1}{\sqrt{2}}(du-ud)c$	$\Sigma_c^{(*)++}$	$\lvert11\rangle$	uuc
$\Sigma_c^{(*)+}$	$\lvert10\rangle$	$\frac{1}{\sqrt{2}}(ud+du)c$	$\Sigma_c^{(*)0}$	$\lvert1-1\rangle$	ddc
Ξ_c^+	$\lvert\frac{1}{2}\frac{1}{2}\rangle$	$\frac{1}{\sqrt{2}}(us-su)c$	Ξ_c^0	$\lvert\frac{1}{2}-\frac{1}{2}\rangle$	$\frac{1}{\sqrt{2}}(ds-sd)c$
$\Xi_c^{\prime(*)+}$	$\lvert\frac{1}{2}\frac{1}{2}\rangle$	$\frac{1}{\sqrt{2}}(us+su)c$	$\Xi_c^{\prime(*)0}$	$\lvert\frac{1}{2}-\frac{1}{2}\rangle$	$\frac{1}{\sqrt{2}}(ds+sd)c$

TABLE IX. The spin wave functions for the charmed hadrons considered in this work.

Hadron	$\lvert Sm_S\rangle$	$\phi^{M_s}_{Sm_S}$	Hadron	$\lvert Sm_S\rangle$	$\phi^{M_s}_{Sm_S}$
				$\lvert11\rangle$	$\uparrow\uparrow$
$\bar{D}/\bar{D}_s$	$\lvert00\rangle$	$\frac{1}{\sqrt{2}}(\uparrow\downarrow-\downarrow\uparrow)$	$\bar{D}^*/\bar{D}_s^*$	$\lvert10\rangle$	$\frac{1}{\sqrt{2}}(\uparrow\downarrow+\downarrow\uparrow)$
				$\lvert1-1\rangle$	$\downarrow\downarrow$
Hadron	$\lvert Sm_S\rangle$	$\phi^{B_s}_{Sm_S}$	Hadron	$\lvert Sm_S\rangle$	$\phi^{B_s}_{Sm_S}$
Λ_c/Ξ_c	$\lvert\frac{1}{2}\frac{1}{2}\rangle$	$\frac{1}{\sqrt{2}}(\uparrow\downarrow-\downarrow\uparrow)\uparrow$	Σ_c^*/Ξ_c^*	$\lvert\frac{3}{2}\frac{3}{2}\rangle$	$\uparrow\uparrow\uparrow$
	$\lvert\frac{1}{2}-\frac{1}{2}\rangle$	$\frac{1}{\sqrt{2}}(\uparrow\downarrow-\downarrow\uparrow)\downarrow$		$\lvert\frac{3}{2}\frac{1}{2}\rangle$	$\sqrt{\frac{1}{3}}(\uparrow\uparrow\downarrow+\uparrow\downarrow\uparrow+\downarrow\uparrow\uparrow)$
$\Sigma_c/\Xi_c^\prime$	$\lvert\frac{1}{2}\frac{1}{2}\rangle$	$-\frac{1}{\sqrt{6}}(\uparrow\downarrow+\downarrow\uparrow)\uparrow+\sqrt{\frac{2}{3}}\uparrow\uparrow\downarrow$		$\lvert\frac{3}{2}-\frac{1}{2}\rangle$	$\sqrt{\frac{1}{3}}(\uparrow\downarrow\downarrow+\downarrow\uparrow\downarrow+\downarrow\downarrow\uparrow)$
	$\lvert\frac{1}{2}-\frac{1}{2}\rangle$	$\frac{1}{\sqrt{6}}(\uparrow\downarrow+\downarrow\uparrow)\downarrow-\sqrt{\frac{2}{3}}\downarrow\downarrow\uparrow$		$\lvert\frac{3}{2}-\frac{3}{2}\rangle$	$\downarrow\downarrow\downarrow$

[1] T. Gershon (LHCb Collaboration), arXiv:2206.15233.
[2] LHCb Collaboration, arXiv:2210.10346.
[3] L. Meng, B. Wang, and S. L. Zhu, arXiv:2208.03883.
[4] R. Aaij *et al.* (LHCb Collaboration), Sci. Bull. **66**, 1278 (2021).
[5] B. Wang, L. Meng, and S. L. Zhu, Phys. Rev. D **101**, 034018 (2020).
[6] F. Z. Peng, M. J. Yan, M. Sánchez Sánchez, and M. P. Valderrama, Eur. Phys. J. C **81**, 666 (2021).
[7] R. Chen, Phys. Rev. D **103**, 054007 (2021).
[8] M. Z. Liu, Y. W. Pan, and L. S. Geng, Phys. Rev. D **103**, 034003 (2021).
[9] C. W. Xiao, J. J. Wu, and B. S. Zou, Phys. Rev. D **103**, 054016 (2021).
[10] J. J. Wu, R. Molina, E. Oset, and B. S. Zou, Phys. Rev. Lett. **105**, 232001 (2010).
[11] E. Santopinto and A. Giachino, Phys. Rev. D **96**, 014014 (2017).
[12] C. W. Shen, J. J. Wu, and B. S. Zou, Phys. Rev. D **100**, 056006 (2019).
[13] C. W. Xiao, J. Nieves, and E. Oset, Phys. Lett. B **799**, 135051 (2019).
[14] J. T. Zhu, L. Q. Song, and J. He, Phys. Rev. D **103**, 074007 (2021).
[15] H. X. Chen, W. Chen, X. Liu, and S. L. Zhu, Phys. Rep. **639**, 1 (2016).
[16] F. K. Guo, C. Hanhart, U. G. Meißner, Q. Wang, Q. Zhao, and B. S. Zou, Rev. Mod. Phys. **90**, 015004 (2018); **94**, 029901(E) (2022).
[17] Y. R. Liu, H. X. Chen, W. Chen, X. Liu, and S. L. Zhu, Prog. Part. Nucl. Phys. **107**, 237 (2019).
[18] L. Meng, B. Wang, G. J. Wang, and S. L. Zhu, arXiv:2204.08716.
[19] H. X. Chen, W. Chen, X. Liu, Y. R. Liu, and S. L. Zhu, arXiv:2204.02649.
[20] X. K. Dong, F. K. Guo, and B. S. Zou, Progr. Phys. **41**, 65 (2021).
[21] T. J. Burns and E. S. Swanson, arXiv:2208.05106.
[22] S. X. Nakamura and J. J. Wu, arXiv:2208.11995.
[23] A. Giachino, A. Hosaka, E. Santopinto, S. Takeuchi, M. Takizawa, and Y. Yamaguchi, arXiv:2209.10413.
[24] M. J. Yan, F. Z. Peng, M. Sánchez Sánchez, and M. Pavon Valderrama, arXiv:2207.11144.
[25] R. Aaij *et al.* (LHCb Collaboration), Phys. Rev. Lett. **122**, 222001 (2019).
[26] R. Aaij *et al.* (LHCb Collaboration), Phys. Rev. Lett. **115**, 072001 (2015).
[27] M. Karliner and J. L. Rosner, Phys. Rev. D **106**, 036024 (2022).
[28] F. L. Wang and X. Liu, Phys. Lett. B **835**, 137583 (2022).
[29] X. W. Wang and Z. G. Wang, Chin. Phys. C **47**, 013109 (2022).
[30] P. G. Ortega, D. R. Entem, and F. Fernandez, arXiv:2210.04465.
[31] K. Chen, B. Wang, and S. L. Zhu, Phys. Rev. D **105**, 096004 (2022).
[32] H. Mutuk, Chin. Phys. C **43**, 093103 (2019).
[33] K. Chen, R. Chen, L. Meng, B. Wang, and S. L. Zhu, Eur. Phys. J. C **82**, 581 (2022).
[34] P. A. Zyla *et al.* (Particle Data Group), Prog. Theor. Exp. Phys. **2020**, 083C01 (2020).
[35] B. Wang, L. Meng, and S. L. Zhu, Phys. Rev. D **101**, 094035 (2020).
[36] L. Meng, B. Wang, and S. L. Zhu, Phys. Rev. C **101**, 064002 (2020).
[37] D. B. Leinweber, A. W. Thomas, and R. D. Young, Phys. Rev. Lett. **92**, 242002 (2004).
[38] P. Wang, D. B. Leinweber, A. W. Thomas, and R. D. Young, Phys. Rev. D **75**, 073012 (2007).
[39] Z. W. Liu, J. M. M. Hall, D. B. Leinweber, A. W. Thomas, and J. J. Wu, Phys. Rev. D **95**, 014506 (2017).
[40] R. Aaij *et al.* (LHCb Collaboration), Nat. Commun. **13**, 3351 (2022).
[41] R. Aaij *et al.* (LHCb Collaboration), Nat. Phys. **18**, 751 (2022).
[42] Z. G. Wang, Int. J. Mod. Phys. A **36**, 2150071 (2021).
[43] H. X. Chen, W. Chen, X. Liu, and X. H. Liu, Eur. Phys. J. C **81**, 409 (2021).
[44] M. L. Du, Z. H. Guo, and J. A. Oller, Phys. Rev. D **104**, 114034 (2021).
[45] K. Azizi, Y. Sarac, and H. Sundu, Phys. Rev. D **103**, 094033 (2021).
[46] R. Chen, Eur. Phys. J. C **81**, 122 (2021).